Formation of self-organized nano- and micro-diamond rings

J. Narayan[1,*], A. Bhaumik[2], S. Gupta[2], P. Joshi[1], P. Riley[1], and R. J. Narayan[2,3]

[1]Department of Materials Science and Engineering, North Carolina State University, Raleigh, North Carolina 27695-7907, USA.

[2] Intel Corporation, Rolner Acres Campus 3, OR, 97124, USA.

[3] Joint Department of Biomedical and Engineering, North Carolina State University and UNC Chapel Hill, Raleigh, North Carolina 27695-7907, USA.

*Corresponding author, Tel: 919-515-7874, E-mail: narayan@ncsu.edu (J. Narayan)

Impact Statement: Significant advancement in the creation of self-organized nanodiamond ring and string structures by laser processing at ambient pressure and temperature

Abstract

We report formation of self-organized nanodiamond ring structures due to dynamical heterogeneity in super undercooled carbon, created by nanosecond laser melting of amorphous carbon layers. We envisage that diamond tetrahedra self-organize and lead to formation of string and ring structures on which nanodiamonds nucleate and grow. Denser ring structures are formed in Q-carbon due to higher undercooling and enhanced diamond nucleation. The average size is larger under heterogeneous nucleation compared to homogeneous nucleation due to lower critical size and free energy, allowing more time for growth. With nanosecond laser melting, growth velocities range 5-10 ms^{-1} and even higher for Q-carbon.

Keywords: Nanodiamond ring; Self-organized nanodiamonds; Q-carbon.

1. Introduction

The formation of self-organized diamond-related nanostructures, which are needed for next-generation quantum technology and nanosensing applications with room-temperature operations, presents tremendous scientific and technical challenges [1,2]. Current equilibrium methods, based upon high-temperature (5000K) and pressure (12 GPa), lead to formation of randomly oriented diamond nanoparticles and microparticles, which cannot be assembled with a fixed orientation on any substrate [1,3]. The chemical vapor deposition (CVD) methods require toxic gases at high temperatures, leading to etching of the substrates and formation of interposing amorphous graphitic layers, which interfere with diamond epitaxy and orientation control [4,5]. The formation of graphitic layers is more prevalent on transition metals and alloys with partially filled d shells, which include most ferrous metals and steels [5]. In addition, the nucleation of diamond by CVD presents challenges for any self-organization and requires external seeding by sprinkling randomly oriented nanodiamonds. This presents challenges for any self-organization and nanodiamonds often are contaminated with unwanted impurities and amorphous carbon layers [6]. Recently, we reported a major breakthrough in the synthesis of diamond and c-BN related materials [7-9], where carbon and BN layers were melted by nanosecond lasers and converted directly into phase-pure diamond and c-BN, respectively. We showed that at a certain undercooling (~1000K), the molten carbon layers converted into diamond, and at a higher values of undercooling a new phase of carbon (Q-carbon) was obtained with many unique and extraordinary properties [8,9]. A detailed analysis of the structure of Q-carbon showed that it consists of diamond tetrahedra, which are packed randomly with a packing efficiency >80%. The bonding characteristics between the tetrahedra were determined to be sp^3 and in between sp^2 with an overall sp^3 content of over 80%. The extraordinary properties of Q-carbon include higher hardness than diamond, room-

temperature ferromagnetism when pure, both n- and p-type doping beyond thermodynamic solubility limit, and record BCS superconductivity in B-doped Q-carbon with transition temperature >55K [7-9].

The primary focus of this paper is that diamond tetrahedra in super undercooled carbon align along <110> or <100> (through 90^0 degree rotation) directions and form strings and rings which provide critical nuclei for diamond growth. Thus, nanodiamonds nucleate and grow more readily around these strings and rings than in the bulk. The number density of clusters of diamond tetrahedra along strings and rings, which provide critical-size diamond nuclei, is much higher in Q-carbon than in α-carbon. This difference leads to a higher number density of nanodiamonds in Q-carbon compared to α-carbon. The α-carbon is formed after quenching the super undercooled state at a lower undercooling than required for Q-carbon. The laser-irradiated area up to one-cm-square-per pulse could be scaled up to 100-200 cm^2s^{-1} by using the 100-200Hz laser. Formation of nanodiamonds and epitaxial nanodots is of special significance in view of many applications ranging from nanoscale imaging to nanosensing, quantum communication, and computing.

2. Experimental

Formation of self-organized nanodiamonds and microdiamond rings required two steps: (1) pulsed laser deposition of amorphous carbon with thickness (50nm-500nm); and (2) laser annealing of amorphous carbon layers to form different diamond microstructures. Amorphous carbon films were deposited using nanosecond laser pulses of a KrF excimer laser (wavelength =248 nm, and pulse duration =25 ns) with chamber pressure of 1.0×10^{-6} to 5.0×10^{-7} Torr at room temperature. The repetition rate and the laser energy density of the nanosecond laser were 10 Hz and 3.0-3.5 Jcm^{-2}, respectively. The ratio of sp^2 to sp^3 bonded carbon of the as-deposited amorphous carbon thin films was controlled by laser and substrate variables, including substrate temperature and

pulse energy density and laser plume characteristics. The amorphous carbon films were laser annealed by using nanosecond ArF excimer laser (wavelength = 193 nm, pulse duration = 20 ns). The Q-carbon was formed in the range of 0.6-0.7 Jcm^{-2} and diamond 0.7-1.0 Jcm^{-2}. The details of the structure and bonding characteristics of different phases have been already published [7-10]. Here, we focus on the formation of self-organized nanodiamond structures.

3. Results and discussions

Amorphous carbon layers can be melted to a super undercooled state by nanosecond laser pulses, and converted upon quenching into diamond-like amorphous carbon with ~60% sp^3 bonding (α-carbon), pure diamond or a new phase of Q-carbon (with ~80% sp^3 bonding). The formation of these phases depends upon the degree of undercooling, where with increasing undercooling α-carbon, diamond and Q-carbon are formed. Fig. 1(a) shows schematically the conversion of amorphous carbon (a-carbon) into graphene, α-carbon, diamond, and Q-carbon near the sapphire substrate, where the undercooling is the highest, followed by diamond and α-carbon layers with decreasing undercooling. The graphene layers are formed, when there is very little or no undercooling. Fig. 1(b) illustrates Gibbs free energy (ΔG_T) versus temperature T, where free energy curves for graphite or graphene (equilibrium phase), and nonequilibrium phases (α-carbon, diamond, and Q-carbon) are intersected by molten carbon with a higher entropy. The formation of different phases occurs at the free-energy intersections, where the degree of undercooling is the difference between the melting point of graphite (~5000K) and melting points of the respective phases.

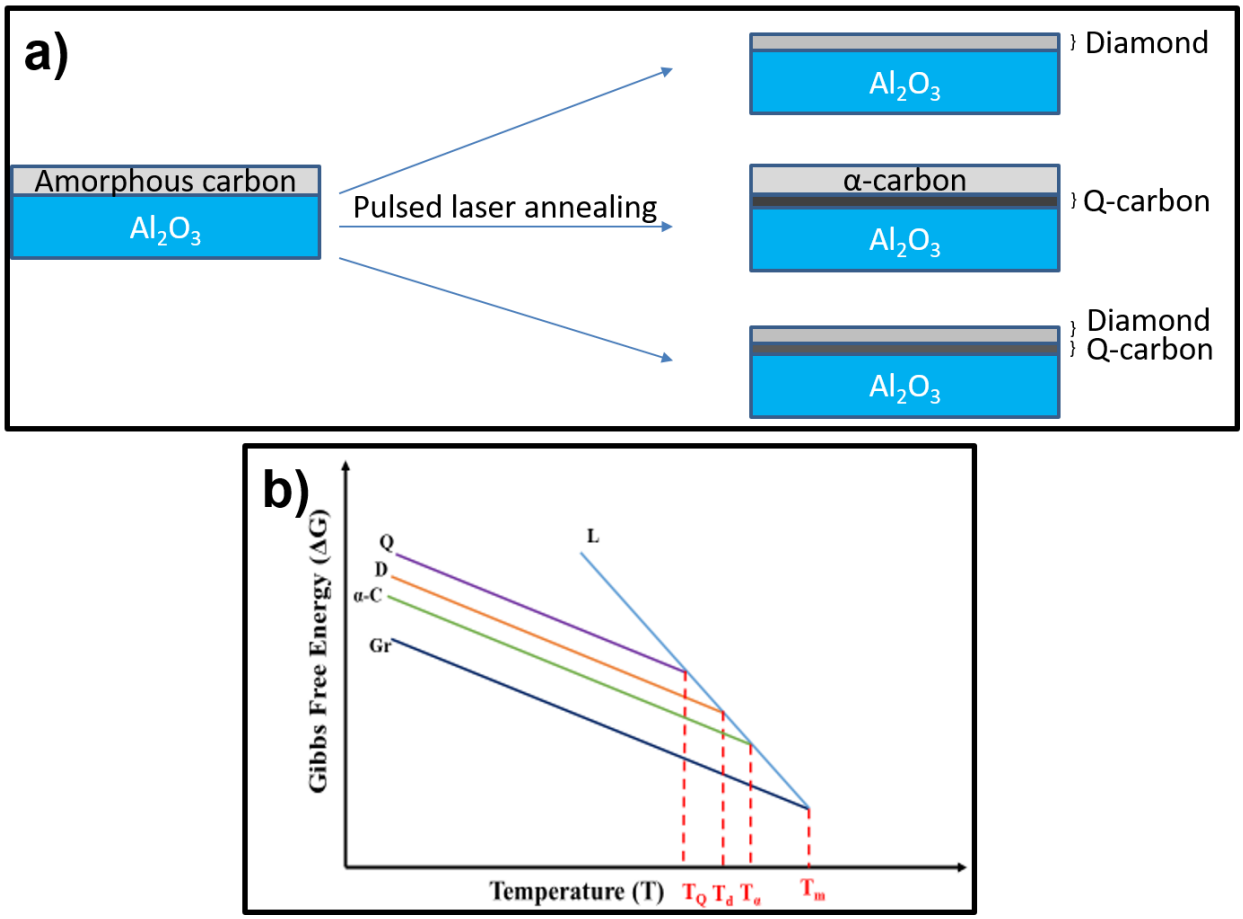

Fig. 1: (a) Conversion of amorphous carbon (a-carbon) into α-carbon, diamond, and Q-carbon near the sapphire substrate; and (b) Gibbs free energy (ΔG_T) versus temperature T, showing temperatures for the formation of different phases.

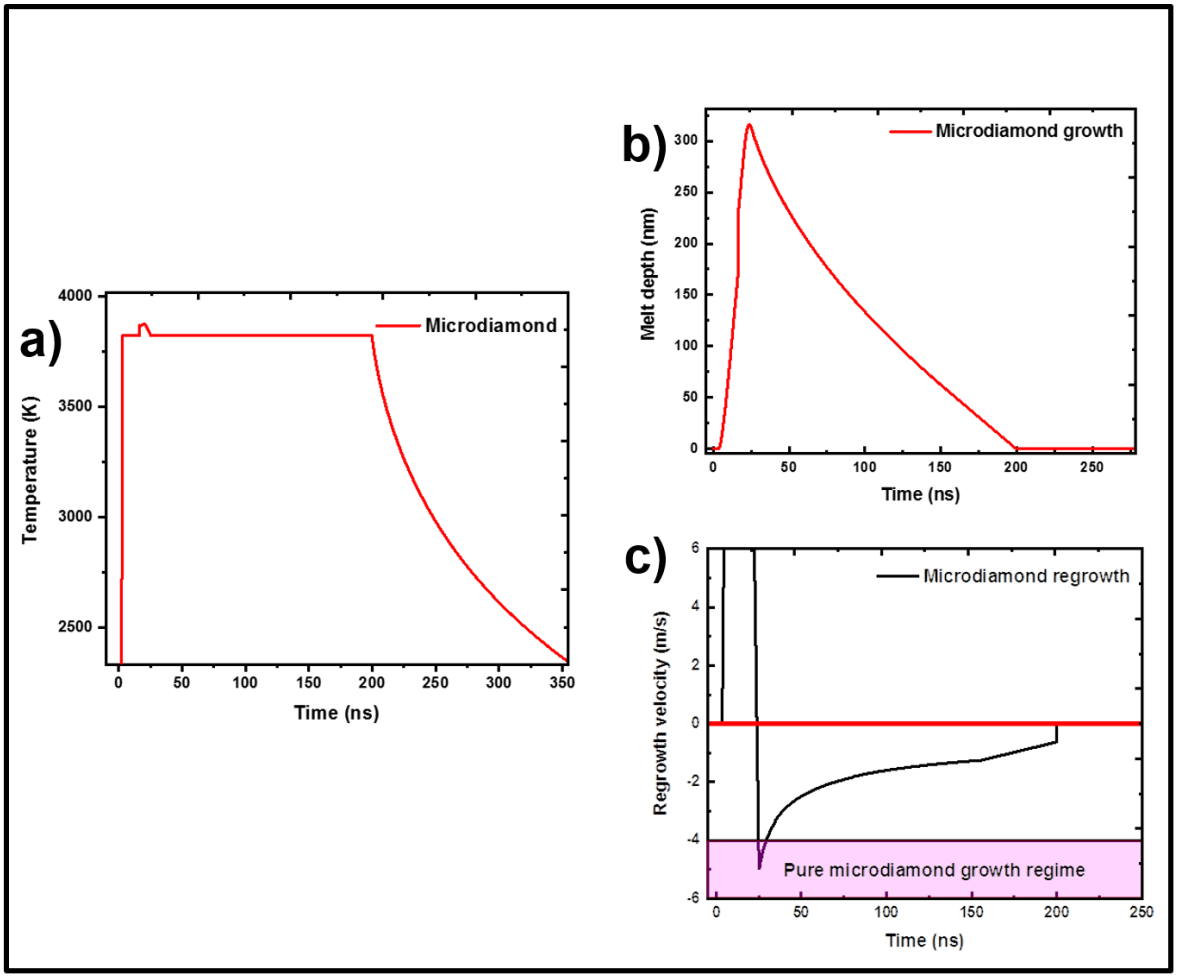

Fig. 2: Laser-solid interaction calculations using the SLIM program: (a) Temperature versus time; (b) Melt depth versus time; and (c) Melt growth velocity as a function of time.

Fig. 2 shows results of laser-solid interaction calculations using the SLIM program [11]. The figure shows the plot of temperature versus time (Fig. 2(a)), melt depth versus time (Fig. 2(b)), and melt growth velocity as a function of time (Fig. 2(c)). The crystal growth velocity for diamond is 3-6 ms^{-1}, and formation velocity for Q-carbon is as high as $10ms^{-1}$. When thin layers of amorphous carbon (a-carbon) are melted to a super undercooled state, it can lead to formation of circular nanodiamond rings at the sapphire interface (R_1), and noncircular nanodiamond rings within the bulk of α-carbon (R_2), as shown in Fig. 3 (a). The strings are formed if the structure is quenched

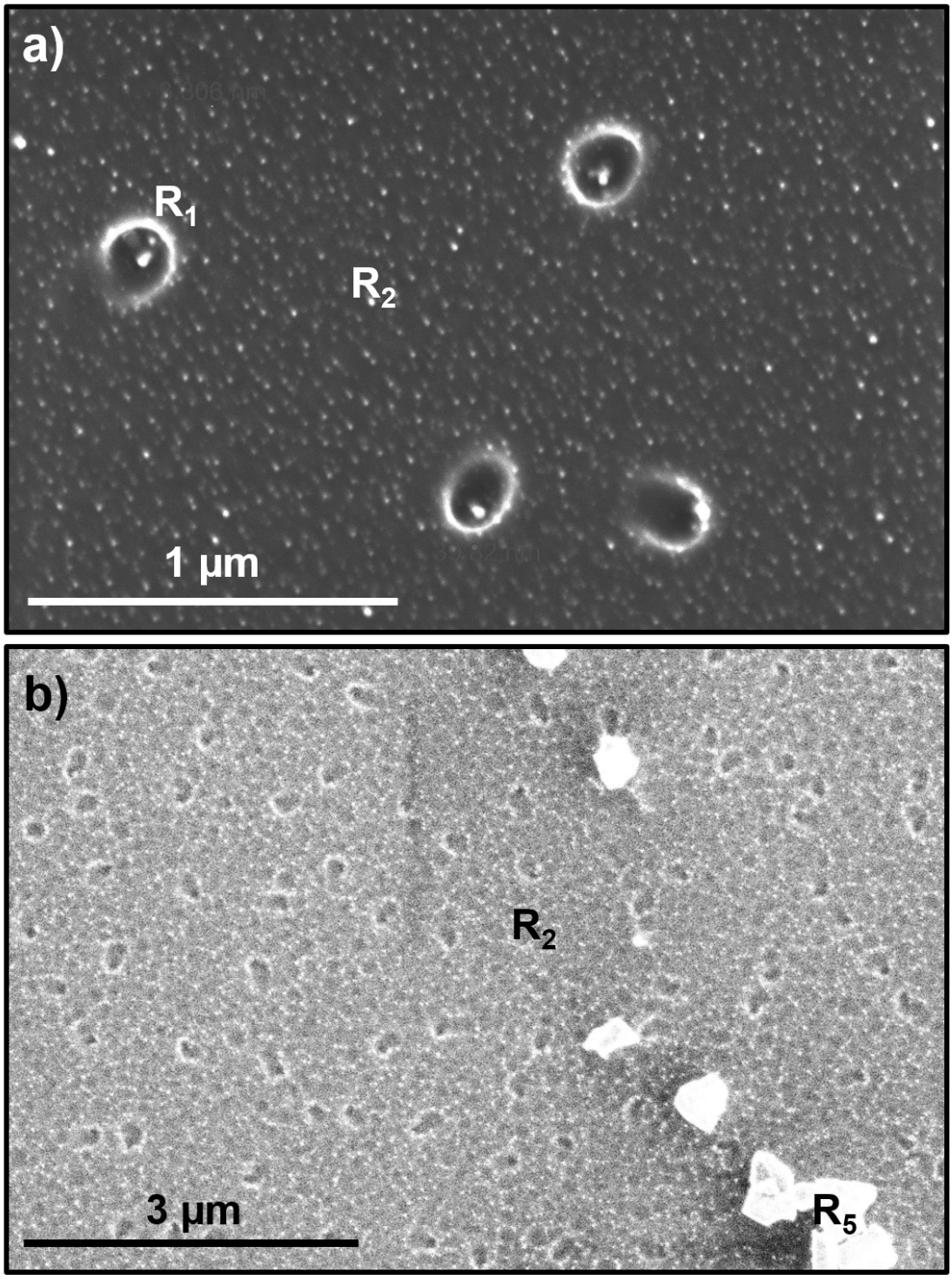

Fig. 3: Formation of circular nanodiamond rings at the sapphire interface (R_1), and noncircular nanodiamond rings within the bulk of α-carbon (R_2); and (b) nanodiamond noncircular rings at the interface and bulk of α-carbon without Q-carbon.

before completing a ring structure. The supplementary Fig. S1 shows schematically the formation of circular nanodiamond rings at the sapphire interface and noncircular rings within the bulk of α-carbon. The noncircular rings are also formed often when two circular rings get merged just before quenching. The nanodiamond formed at the sapphire interface anchors the ring formed in α-carbon, as illustrated in Fig. S1. The lighter contrast associated with the circular nanodiamond rings in direct contact with sapphire is attributed to a charge build-up during HRSEM imaging [12]. The nanodiamonds associated with noncircular rings within the bulk of α-carbon do not show such a contrast, except for those on the sapphire. The number density of nanodiamonds at R_1 on the sapphire is much higher compared to R_2, because of the heterogeneous nucleation and the presence of Q-carbon near the sapphire interface. The higher undercooling near the interface increases the gain in Gibbs free energy and reduces the critical diamond nucleus size. The Gibbs free energy is given by $\Delta G_T = -\Delta H_m . \Delta T/T_m$, where ΔT is the undercooling, ΔH_m melting enthalpy, and T_m is the melting point of carbon. The atomic structure of Q-carbon provides critical size diamond nuclei on which nanodiamonds grow readily. Fig. 3(b) shows nanodiamond rings associated with melt puddles at the sapphire interface and within the bulk of α-carbon (R_2). In addition, the figure shows the formation of epitaxial <111> microdiamonds which grow on (0001) sapphire template (R_5). These results provide a direct evidence for the formation of rings and strings as a result of large undercooling in the molten carbon. The details of this growth will be discussed later in this paper.

Fig. 4 (a) shows formation of circular and noncircular rings with high density of nanodiamonds in Q-carbon (R_1), where noncircular rings are formed when two circular rings merge before quenching. The details of noncircular nanodiamond rings within the bulk of α-carbon are illustrated at R_2, which grow in conjunction with larger nanodiamonds having lighter contrast at

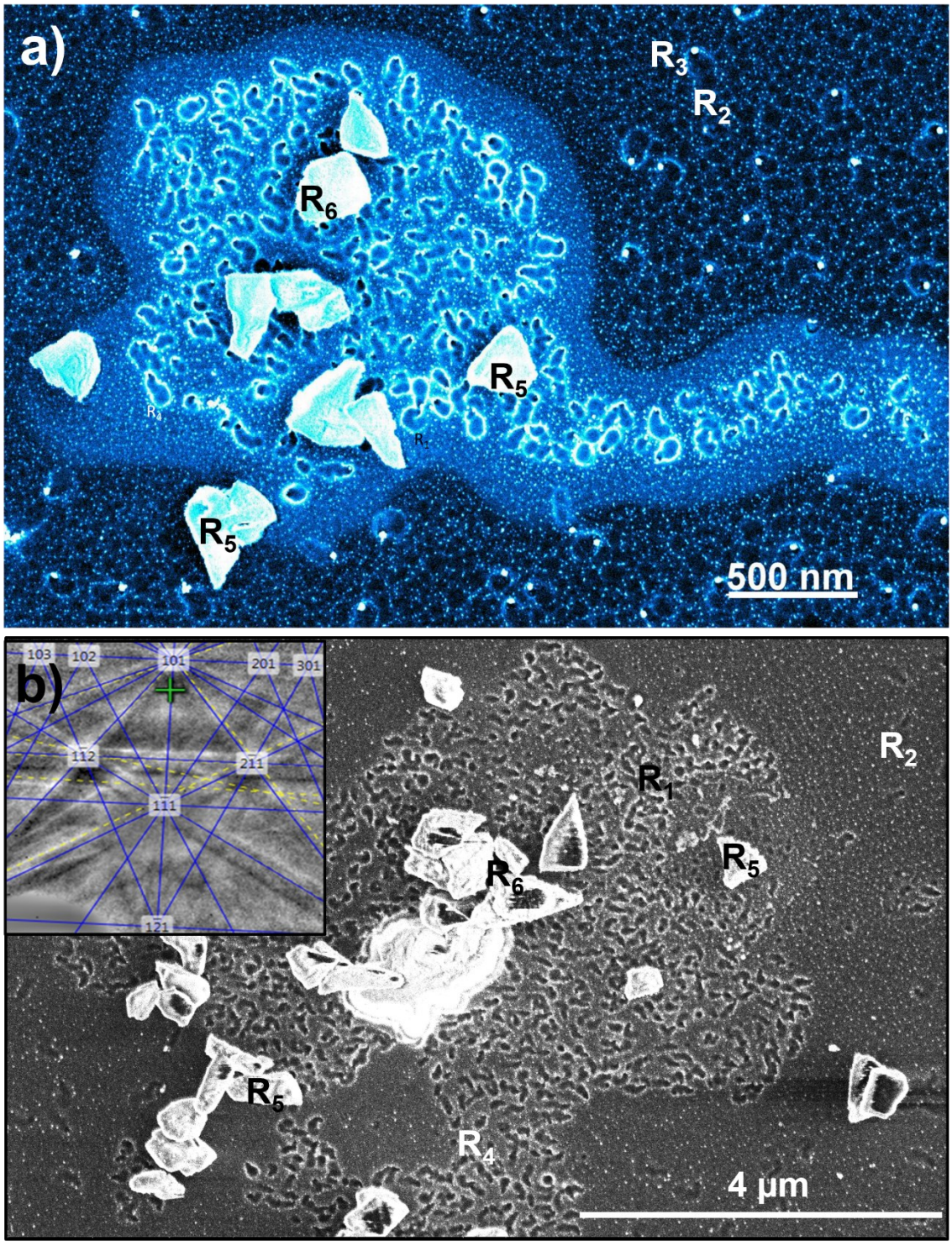

Fig. 4: (a) Direct comparison of nanodiamond rings and epitaxial microdiamonds in α-carbon and Q-carbon, and (b) Different morphology nanodiamond rings and epitaxial microdiamonds in α-carbon and Q-carbon. The inset shows <111> diamond EBSD pattern from R_5.

R_3 on the sapphire substrate. These larger nanodiamonds grow directly on the sapphire substrate via heterogeneous nucleation. This figure shows a large area of Q-carbon and α-carbon, where growth of nanodiamond rings and epitaxial microdiamonds can be clearly compared. It is interesting to note that the number density of nanodiamonds in rings associated with Q-carbon (R_4) is considerably higher than that in the α-carbon (R_2). This is surmised to result from the presence of a much higher number density of critical size diamond nuclei in Q-carbon. Fig. S2 illustrates the formation of these three different microstructures schematically. The average size of nanodiamonds in Q-carbon and in α-carbon is about the same (5nm), implying that both phases have diamond nuclei of critical size [13, 14], however, number density of these nuclei is much higher in Q-carbon than in the α-carbon. This micrograph shows the growth of <111> microdiamonds (R_5) and <100> microdiamond (R_6) with sapphire 0001) substrate in both α-carbon and Q-carbon regions. Fig. 4 (a) also shows a direct comparison of morphologies of nanodiamond rings and growth of microdiamonds in Q-carbon and α-carbon. The <111> diamond epitaxial growth at R_5 is confirmed by the inset EBSD pattern in Fig. 4(b). The epitaxial growth of diamond on (0001) sapphire is found to have mostly triangular (<111> epitaxy at R_5), but some rectangular morphology (<100> epitaxy at R_6). These <111> oriented microdiamonds at R_5 and <100> microdiamonds at R_6 grow with respect to sapphire via domain matching epitaxy [DME][15]. The epitaxial relation at R_5 was determined to be <111> Diamond // <0001> Sapphire out of the plane, and $<\bar{1}10>$ Diamond // $<\bar{2}110>$ Sapphire in the plane via DME. The DME involves matching of eighteen $(\bar{2}110)$ half planes of sapphire with seventeen (110) planes of silicon. The epitaxial relation at R_6 was determined to be <100> Diamond // <0001> Sapphire out of the plane, and $<\bar{1}10>$ Diamond // $<\bar{2}110>$ Sapphire in one direction and $<\bar{1}10>$ Diamond // $<\bar{1}0\bar{1}0>$ Sapphire in the other direction on the plane, which involves a $30^0/90^o$ rotation. Along the $<10\bar{1}0>$ direction,

eleven $(10\bar{1}0)$ half planes of sapphire with twelve (110) planes of diamond. It is interesting to note that average size of these microdiamonds (at R_5 and R_6) is about 250nm, from which diamond growth velocity is estimated 5.0 ms^{-1} by using 50ns growth estimated from SLIM calculations [11]. It should be mentioned that the nucleation of diamond on sapphire substrates is quite challenging by CVD processes due to lack of nucleation sites and presence of carbide forming interfacial layers [6]. Fig. 4(b) shows a different morphology of formation of nanodiamond rings in Q-carbon at R_1 and in α-carbon at R_2, and <111> and <100> epitaxial microdiamonds on sapphire substrate at R_5 and R_6, respectively. The inset shows <111> EBSD diamond pattern to confirm epitaxial growth on sapphire. It is interesting to note that <100> epitaxy of diamond is possible on (0001) sapphire, when there is <110> Diamond//$<\bar{2}110>$ Sapphire in one direction and $<\bar{1}10>$ Diamond//$<\bar{1}010>$ Sapphire in other direction of the film plane. Fig. S3 shows Raman spectra from nanodiamonds, where diamond T_{2g} peak is shifted slightly downwards (~5cm^{-1}) from bulk diamond peak at 1332cm^{-1} to illustrate quantum confinement effects.

The formation of a perfect Q-carbon micro-ring structure occurs by generation of a wave pattern (puddles) in the super undercooled molten carbon, where a thickness variation [16] leads to formation of Q-carbon at the troughs. This is illustrated schematically in Fig. S4. At a lower thickness, the undercooling is optimized for the formation of Q-carbon. Fig. 5(a) shows formation of Q-carbon ring structure with 5-7 microns diameter (r_1). When these Q-carbon rings merge, they create larger and more complex structures. When these ring structures just touch, there are larger Q-carbon and diamond structures at the boundary (r_2). However, if these ring structures meet before Q-carbon and diamond nucleation, then there is no residual boundary between them (r_3). When multiple ring structures meet, they create highly complex shapes, as shown at r_4. The most interesting observation was the formation of diamond ring structures within the Q-carbon phase,

as shown at a higher magnification in Fig. 5 (b) at r_5. Fig. 5(b) shows the formation of different nanodiamond ring structures within a Q-carbon ring structure with average nanodiamond size of 5-10nm. These nanodiamonds grow on sapphire (0001) epitaxially via DME.

The formation of diamond ring structures within Q-carbon rings (Fig. 5(b)) occurs at a slightly lower undercooling. The formation of diamond ring structure is periodic, similar to that observed earlier in nanodiamond rings from super undercooled carbon. The periodic structures are formed as a result of periodic thickness fluctuations which lower the total free energy. The formation of wave pattern on the surface of molten super undercooled carbon is caused by surface tension instability, which leads to formation Q-carbon ring structures. The formation of nanodiamond ring structure is caused by line tension instability around the ring, where periodic nanodiamond structure may lead to a lower free energy.

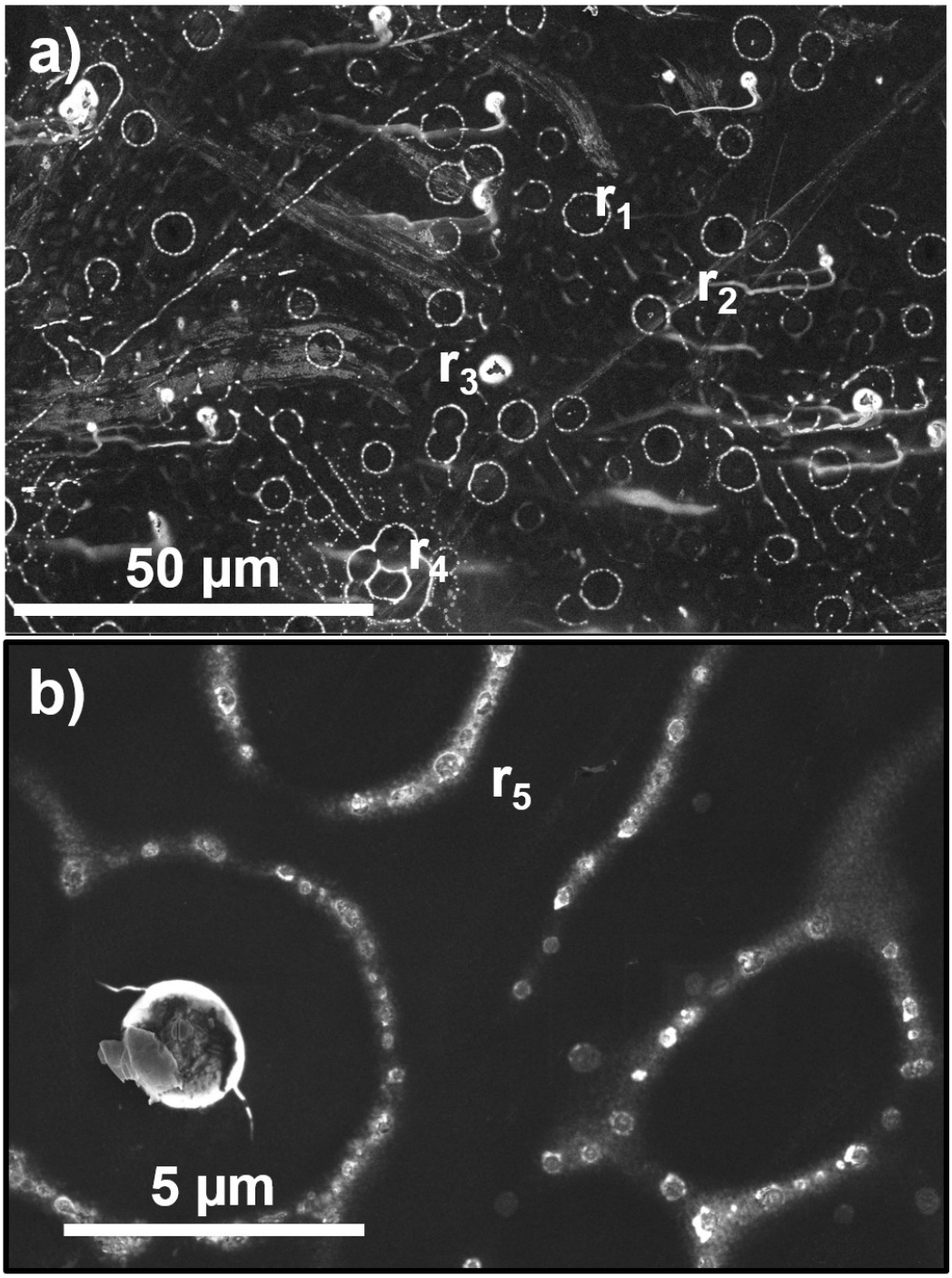
a)
r1
r2
r3
r4
50 µm
b)
r5
5 µm

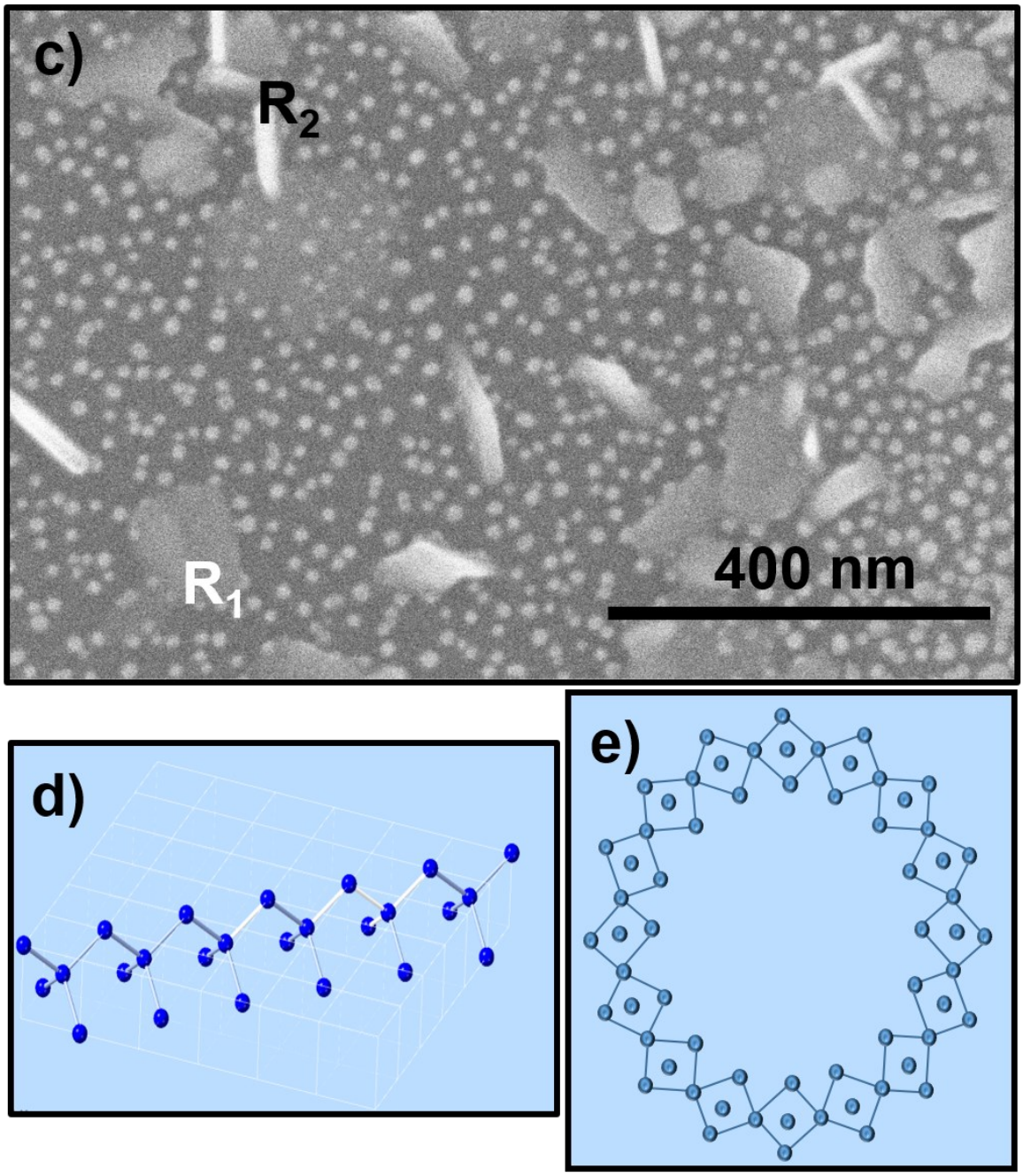

Fig. 5: (a) Formation of large circular microrings with the sapphire substrate; (b) Formation of nanoring structure within the microrings;(c) Formation of self-organized epitaxial nanodiamonds at the α-carbon/sapphire interface; (d) Schematic representation of alignment of diamond tetrahedra along the <110> directions for the formation stringlike structures; and (e) Self-organization of <110> strings into circular rings to minimize line tension energy.

Formation of self-organized nanodiamonds is shown in Fig. 5(c) at the α-carbon/sapphire interface. Here the nanodiamonds grow epitaxially with <111> diamond//<0001> sapphire by domain matching epitaxy with the in-plane alignment of <110>diamond//<$\bar{2}$110>sapphire. Fig. S5 shows the formation of self-organized epitaxial nanodiamonds and microdiamond platelets on a (0001) sapphire substrate. It is interesting to note the presence of diamond plates growing parallel (at R_1), in addition to plates normal to the (0001) sapphire substrate (at R_2). It is envisaged that the nucleation of platelets is associated with the formation of a thin layer of Q-carbon, where subsequent growth is dictated by these nuclei. When the Q-carbon layer breaks into small filamentary structures like nanorods, then these provide nucleation sites to grow platelet structures normal to the substrate. By doping amorphous carbon layers with N and Si, nanodiamonds can be doped with N and Si to create NV and SiV doped nanodiamonds needed for quantum sensing, communication, and computing [17].

The formation of strings and rings in α-carbon and Q-carbon is rationalized by the alignment of diamond tetrahedra along the <110> directions, as shown in Fig. 5(d). The alignment of diamond tetrahedra along <100> directions requires a 90^0 rotation between two adjacent tetrahedra. This alignment can result from dynamical heterogeneity, which has been studied experimentally and theoretically in supercooled liquids and spin glasses [18, 19]. The formation of stringlike structure is found to increase with undercooling as we go from α-carbon to Q-carbon. These <110> strings can self-organize into rings to minimize line tension energy, as shown in Fig. 5(e). The diamond tetrahedra along these strings and rings provide critical nuclei for diamond formation. The size of the nanodiamonds along these rings is determined by the pulse duration and available time for liquid-phase growth during the quenching cycle. The separation between nanodiamonds is considerably lower in Q-carbon than in α-carbon, while the average size is about the same. This

may result from higher undercooling in Q-carbon than in α-carbon. The formation of Q-carbon has been confirmed theoretically [20] and experimentally [21] by other researchers.

The Q-carbon structure consists of randomly packed diamond tetrahedra with packing efficiency >80%. The bonding within the tetrahedra is sp^3 with sp^2 bonding between tetrahedra. The diamond tetrahedra provide easy nucleation sites for diamond growth. When three diamond tetrahedra then get together in the form of a string (as in Q_1 phase), it may achieve a critical diamond nuclei for homogeneous nucleation, estimated to be ~1nm [7]. The Q_1 phase is formed when three diamond tetrahedra units are repeated randomly [9]. We have shown the formation of three distinct Q phases in B-doped Q-carbon (namely QB_1, QB_2, and QB_3) with superconducting transition temperature of 37K, 57K, and over 110K, respectively [9]. The diamond ring structure is formed at a lower undercooling, with a smaller number density per unit length than at Q-carbon undercooling, where nucleation density is much higher because of higher density of carbon tetrahedral packing.

4. Summary

We have shown the formation of self-organized nanodiamond structures by nanosecond laser melting of carbon layers followed by rapid quenching. Nanodiamond structures are formed within the bulk as a result of dynamical heterogeneity that occurs in super undercooled carbon by homogeneous nucleation, and at the film-substrate interface by heterogeneous nucleation. In the case of heterogeneous nucleation, nanodiamonds and microdiamonds grow epitaxially via domain matching epitaxy on the sapphire substrate. The nucleation of diamond is substantially enhanced in the presence of Q-carbon, as the number density of clusters of diamond tetrahedra with critical nuclei sizes is much higher in the Q-carbon phase. These results provide a direct evidence for dynamical heterogeneity in super undercooled carbon.

Disclosure statement

No potential conflict of interest was reported by the author(s).

Acknowledgment

We are pleased to acknowledge useful discussions and comments by Professor John Prater at NCSU. This work was supported by the National Science Foundation Grant (DMR-2016256).

References:

1. Das D, Singh RN. A review of nucleation, growth and low temperature synthesis of diamond thin films, Int. Mater. Rev. 2007;52:29–64.

2. Nebel CE, Rezek B, Shin D, et al. Diamond for bio-sensor applications, J. Phys. D. Appl. Phys. 2007;40:6443–6466.

3. Bundy FP, Bassett WA, Weathers MS, et al. The pressure-temperature phase and transformation diagram for carbon; updated through 1994, Carbon. 1996;34:141–153.

4. Angus JC, Hayman CC. Low-pressure, metastable growth of diamond and "diamondlike" phases, Science. 1988;241:913–921.

5. Chen X, Narayan J. Effect of the chemical nature of transition-metal substrates on chemical-vapor deposition of diamond, J. Appl. Phys. 1993;74:4168–4173.

6. Singh RK, Gilbert DR, Fitz-Gerald J, et al. Engineered Interfaces for Adherent Diamond Coatings on Large Thermal- Expansion Coefficient Mismatched Substrates, Science. 1996;272:396–398.

7. Narayan J, Bhaumik A. Novel phase of carbon, ferromagnetism, and conversion into diamond, J. Appl. Phys. 2015;118.; US Patent # 10,566,193 (2019).

8. Narayan J, Bhaumik A, Gupta S, et al. Progress in Q-carbon and related materials with extraordinary properties, Mater. Res. Lett. 2018;6:353–364.

9. Narayan J, Bhaumik A, Sachan R: High temperature superconductivity in distinct phases of amorphous B-doped Q-carbon, J. Appl. Phys. 2018; 123 135304.

10. Sachan R, Hachtel JA, Bhaumik A, et al. Emergence of shallow energy levels in B-doped Q-carbon: A high-temperature superconductor, Acta Mater. 2019;174:153–159.

11. Singh RK, Narayan J. A novel method for simulating laser-solid interactions in semiconductors and layered structures, Mater. Sci. Eng. B. 1989;3:217–230.

12. Kim KH, Akase Z, Suzuki T, et al. Charging Effects on SEM/SIM Contrast of Metal/Insulator System in Various Metallic Coating Conditions, Materials Transactions. 2010;51:1080-1083.

13. Wood RF, Lowndes DH, Narayan J: Bulk nucleation and amorphous phase formation in highly undercooled molten silicon, Appl. Phys. Lett. 1984;44:770–772.

14. Lowndes DH, Wood RF, Narayan J: Pulsed-Laser Melting of Amorphous Silicon: Time-Resolved Measurements and Model Calculations, Phys. Rev. Lett. 1984;52:561–564.

15. Narayan J, Larson BC. Domain epitaxy: A unified paradigm for thin film growth, J. Appl. Phys. 2003;93:278–285.

16. Narayan J, Wang H, Choi HK, Fan JCC, Effect of thickness variation in high-efficiency InGaN/GaN light-emitting diodes, Appl. Phys. Lett. 2002; 81: 841-843.

17. Narayan J, Bhaumik. A. Novel Synthesis and Properties of Pure and NV-Doped Nanodiamonds and Other Nanostructures, Mater. Res. Lett. 2017; 5:242-250.
18. Donati C, Douglas JF, Kob W, et al. Stringlike cooperative motion in a supercooled liquid, Phys. Rev. Lett. 1998;80:2338–2341.
19. Gebremichael Y, Vogel M, Glotzer SC, Particle dynamics and the development of string-like motion in a M monoatomic supercooled liquid, J. Chem. Phys. 2004;120:4415–4427.
20. Sakai Y, Chelikowsky JR, Cohen ML: Simulating the effect of boron doping in superconducting carbon, Phys. Rev. B. 2018;97.
21. Yoshinaka H, Inubushi S, Wakita T, et al. Formation of Q-carbon by adjusting sp^3 content in diamond-like carbon films and laser energy density of pulsed laser annealing, Carbon. 2020;167:504–511.